Fluid flow and colloid transport experiment in single-porosity sample; tracking of colloid transport behavior in a saturated micromodel

Enno T. de Vries [a,*], Qianjing Tang [a], Sanli Faez [b], Amir Raoof [a]

[a] *Department of Earth Sciences, Utrecht University, the Netherlands*
[b] *Nanophotonics, Debye Institute for Nanomaterials Research, Utrecht University, the Netherlands*

ARTICLE INFO

ABSTRACT

Release of colloids and their subsequent transport into the subsurface environments takes place during a wide range of applications such as industrial, energy storage, and agricultural activities. Therefore, processes contributing to transport, attachment, and re-mobilization of colloids in porous media are attracting attention. A fraction of the released colloids may cross the soil vadose zone to reach the saturated groundwater. In this study, we explored colloid transport in a micromodel with high repulsion energy barrier where colloid retention is assumed to be low. Three major shortcomings were improved: pore space domain size, imaging resolution, and speed of imaging. The flow path of 1357 colloids with a size of 4 μm were tracked and these enabled precise determination of individual colloid transport mechanism as well as the integrated behavior of the system.

Our direct observations have shown that even under unfavorable attachment conditions (defined based on the DLVO theory) colloids deposition occurred which was mainly due to the local flow velocity fluctuations and grain surface heterogeneity. Using the information from collective trajectories, we have quantified the contribution of differently behaved colloids in the observed breakthrough curve which show an integrated, macroscopic, behavior of the system and is often the only available information when performing column or field scale experiments to explore colloid transport in porous media. Furthermore, we have shown that attachment and remobilization of colloids increased the dispersion coefficient, and consequently the dispersivity value of the media.

1. Introduction

The increased use of natural and engineered colloids and nanoparticles in agriculture, industry, and consumer products lead to more exposure of soils to these particles (Kretzschmar et al., 1999; Troester et al., 2016; Wang et al., 2016). Moreover, in the recent years the subsurface environment is being extensively used for energy storage applications which promote creation and remobilization of colloids. Particle transport in the subsurface is therefore attracting much attention since particles are now being detected in larger amounts in the environment, including in drinking water supplies, which can pose health threats (Kretzschmar and Schafer, 2005; Rodrigues et al., 2016; Zhou et al., 2017). The vadose zone of soil generally acts as a natural barrier against groundwater pollution. Therefore, the groundwater is less prone to pollution than the surface water due to natural attenuation processes taking place in this section of the earth. However, once contaminated, pollution in groundwater can remain for very long

periods of time, with groundwater remediation often being very complicated (Troester et al., 2016). Although a large fraction of pollutants may be filtered out by the vadose zone, more intense land usage causes more pollution of groundwater (i.e., the saturated zone) where contaminants can be transported and spread relatively fast. The subsurface is often very heterogeneous chemically and physically(Argent et al., 2015; Bradford et al., 2015), with the transport of colloids being affected by several coupled processes (Mitropoulou et al., 2013; Sang et al., 2013). Therefore, predicting the final state and transport of colloids in the subsurface is very complicated and requires a fundamental understanding of the main governing processes.

For surfaces with opposite charges, particle deposition is favorable because van der Waals and electric double layer type interactions are both attractive, which allows colloid transport to be well-predicted using colloid filtration theory, CFT (Yao et al., 1971; Baumann and Werth, 2004; Massoudieh and Ginn, 2010). Using CFT, the removal of particles from the bulk fluid can be calculated with a single collector

---

efficiency. However, when the two surfaces are similarly charged (which is often encountered in the earth subsurface), electric double layer interactions are repulsive while van der Waals interactions attractive. An energy barrier against deposition can develop under these electrostatically unfavorable conditions. In that case, an extra parameter, defined as the attachment efficiency, is employed to account for the repulsive forces (Tufenkji and Elimelech, 2004; Miele et al., 2019). To determine the various parameters, colloid transport experiments are often caried out at the column length scale (Syngouna and Chrysikopoulos, 2015), from which colloid breakthrough curves are obtained at the column exit. Empirical absorption coefficients can be estimated by fitting the breakthrough data using macroscopic formulations (Molnar et al., 2015). The Derjaguin-Landau-Verwey-Overbeek (DLVO) theory may be used to determine the net-interaction energy between a collector surface and a colloid, or between colloids by combining van der Waals attraction forces and the electrostatic repulsion forces (Ryan and Elimelech, 1996; Peng et al., 2010). The theory assumes smooth surfaces with uniform chemical properties, although the approach does not consider local roughness (Argent et al., 2015) and local surface charge fluctuations that may happen due to chemical nonuniformities (Bradford et al., 2015). Spatial variability in the pore water velocity is also known to affect colloid transport of colloids, which is not included in the DLVO theory.

A wide range of adsorption processes act on colloids (e.g., straining, bridging, electrostatic interaction, and aggregation), with their occurrence and frequency depending on the dynamics of flow and the surface properties (Bradford and Torkzaban, 2015). These processes interact with the spatially variable pore velocities to ultimately affect the attachment and remobilization of colloids. Observing such interactions requires relatively large samples where pore sizes and pore connectivity are considered to capture both velocity variations and the occurrence of different adsorption processes. However, large domain sizes together with the required imaging resolution to observe individual colloids provide major challenges for direct observations of colloid transport in porous media and therefore upscaling of colloid transport in porous media. These challenges produce much uncertainty in linking the observed colloid breakthrough curves obtained to the basic processes (Wang et al., 2012; Bradford and Torkzaban, 2015; Molnar et al., 2015). To overcome these difficulties, pore-scale experiments should be performed where colloid transport, adsorption, and mobilization can be observed directly and simultaneously within a sufficient number of pores to accurately represent the target porous medium. So far, for porous media in the size ranges of sand (i.e., grain sizes of around 100 μm), direct observations have been carried out using microscopy methods such as confocal scanning microscopy (Lazouskaya et al., 2011, 2013; Zhang et al., 2013). These methods provide micrometer-scale observations, however for relatively small domain sizes. The imaged domain sizes then often cover one pore or even smaller (e.g., part of a pore located close to the collector surface). Local roughness and flow field variations between different pores in that case are left out when using single flow channels (Lazouskaya et al., 2011; Sun et al., 2018), capillary tubes, or in case of using limited number of pores or regular/periodic pore structure (Auset and Keller, 2006a; Wang et al., 2011; Liu et al., 2019). Periodicity in porous media is known to lead to a dependency on the direction of the flow with respect to the periodicity of the medium (Nguyen et al., 2017; Reichhardt and Reichhardt, 2021).

In this study, we investigated colloid transport under unfavorable conditions using realistic pore structure composed of a large number of pores. Meanwhile, the whole pore structure together with all individual colloids are imaged simultaneously and over time. We developed for this purpose an optical set-up allowing to image the micromodel with a resolution of 2.9 μm, using a micromodel with a length and width of 10 mm with an irregular pore structure, and a frame rate of 10 frames per second to track colloid trajectories. The transport paths of the colloids, involving a total of over 1300 separate trajectories within the domain, were further categorized into three groups of colloids: i-mobile colloids, ii-immobilized colloids, and ii-remobilized particles. Transport

properties of each category, and then analyzed in detail. The main goal is to capture the full trajectory of colloids flowing through the pore network and observe their dynamic behavior in the presence of a high repulsion energy barrier where retention is presumed to be low.

2. Materials and methods

2.1. Pore space topology

In this study, we used real pore structures obtained by 3D imaging a sand sample using x-ray tomography. The 3D image was used to extract a 2D slice to develop a mask needed to fabricate a polydimethylsiloxane (PDMS) micromodel. The pore structures were fabricated using soft lithography techniques. The pore domain had a physical size of 10×10 mm^2, and the full micromodel (including the inlet and the outlet structures) had a size of 25×10 mm^2 with a depth of 20 μm and a porosity of 0.40. The micromodel allows for direct observation of colloid transport, although due to the quasi-2D structure grain-grain contacts are present although they do not accurately represent the contact points of a 3D porous media. Fig. 1 shows the complete micromodel structure, with Table 1 providing details of the solid phase and the pore space. Detailed information is provided in the Supplementary Materials.

2.2. The microscopy setup and the experimental procedure

We developed a home-build microscope setup to perform particle tracking. The setup consisted of two 595 nm LED's (Thorlabs M595) with band-pass filters of 580 ± 10 nm (Thorlabs FB580–10) to excite the colloids (Fig. 2). We used 4-μm colloids (FluoSpheres™ Sulfate Microspheres (580/605), ThermoFischer) which emitted red light at a peak wavelength of 605 nm. The emitted light was isolated and captured using a long-pass filter of 600 nm (Thorlabs FEL0600) placed in front of the camera (Basler acA5472–17um). Fluid flow was established using a syringe pump (Harvard Apparatus Pump 11 Pico Plus Elite) connected by a tube to the micromodel main inlet channel. The main outlet channel was connected to a fluid reservoir. Fig. 2 provides the configuration of the setup.

The pore space is initially fully saturated with ethanol. Afterward, we injected 100 pore volumes (PV) of colloid-free water into the pore space to provide fully saturated water flow and steady state condition. The experiment was continued by injecting 5 PV of the solution containing colloids followed by 10 PV of a colloid-free solution at an average pore-water velocity of 12.0 m day^{-1}. A low input concentration was used to stay in the single-colloid limit which is usually the case in the earth subsurface environment such as transport of pathogenic bacteria and viruses where they are present under low concentrations to increase their survival chances for long time periods of several months (Pekdeger and Matthess, 1983; Schijven and Hassanizadeh, 2000). Under such low concentrations, clogging and plugging of pores does not happen due to bridging and straining processes, unlike other studies that focus on clogging of porous media under relevant conditions (Auset and Keller, 2006b; Reichhardt and Reichhardt, 2017; Péter et al., 2018; Parvan et al., 2021). Accurate imaging required minimum disturbance and vibration of the setup during the injection experiments. To achieve this, the complete sequence of solutions (i.e., the sequence of clean solutions and solutions having colloids) were injected prior to the start of experiments into the inlet tube. This approach allowed different target solutions to enter the micromodel without changing the tubing of the system or using any flow switch which can affect the accuracy of injection and imaging. Throughout the experiment images were recorded at a resolution of 2.9 μm with an imaging rate of 10 frames per second.

2.3. The imaging processes

An image of a fully rhodamine saturated micromodel was taken to serve as the reference image (mask) for the pore space during analyses.
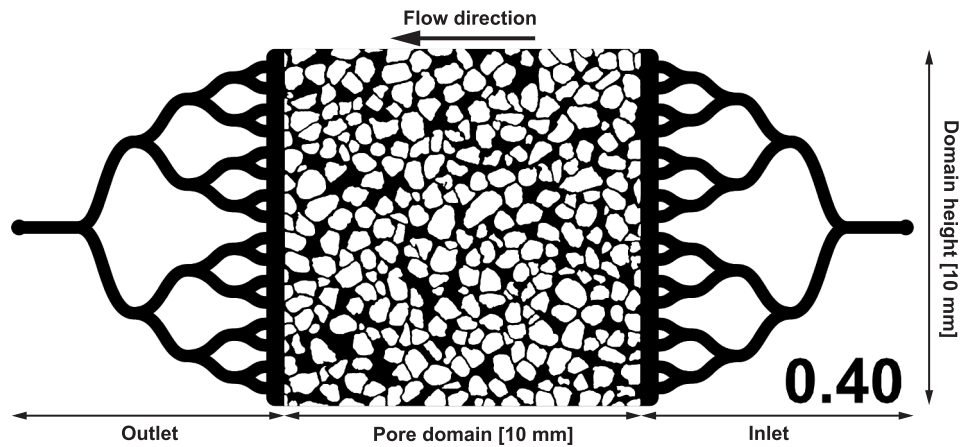
Fig. 1. Micromodel structure including inlet and outlet structures designed to provide an even distribution of fluid flow and colloids entering the domain during the experiment.

Table 1
Information about the solid phase and pore space of the micromodel.

	Property	Value
solid phase	Number of grains	317
	Grain diameter [mm]	0.473 (0.144)*
	Grains shape factor [−]	0.811
pore space	Number of pore bodies	460
	Number of pore throats	708
	Pore body diameter [mm]	0.324 (0.092)*
	Pore throat diameter [mm]	0.145 (0.063)*
	Pore shape factor [−]	0.435 (0.133)*

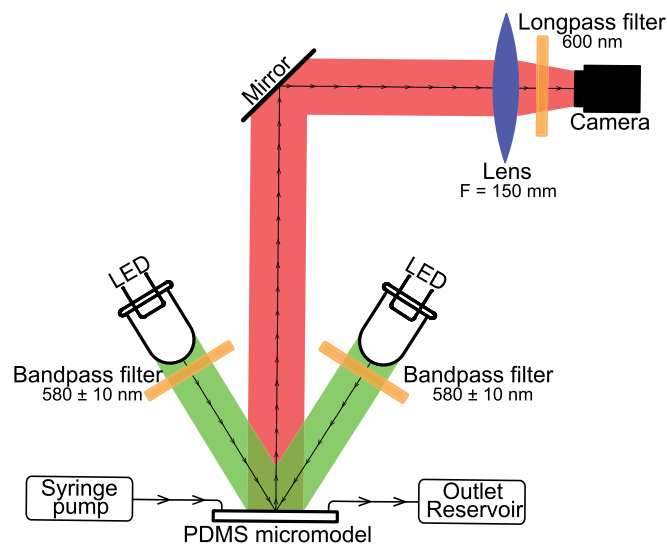*values in parenthesis indicate standard deviations.

Fig. 2. Schematic of the microscopy set-up: two green LED's (Thorlabs M595) with bandpass filters of 580 ± 10 nm were used to excite the colloids. The emitted red light by colloids, with a peak wavelength of 605 nm, was isolated using a long-pass filter of 600 nm. Images are captured with a Basler acA5472–17um using a frame rate of 10 frames per second.

Comparisons of images taken during the experiments against the reference image provides images of only the pore space, including the colloids. We used image analysis to detect colloids within each individual image and tracking individual colloids between successive frames (i.e.,

one-to-one paring of colloids in each frame n to colloids in a successive frame $n + 1$) to obtain complete colloid trajectories. Laplacian of Gaussian particle detection (LoG detector) was used to detect particles (Lindeberg, 1998), and the Linear Assignment Problem (LAP) particle-linking algorithm (Jaqaman et al., 2008), applied in the TrackMate package developed by Tinevez et al. (2017), for our experiments as it is optimized for non-dense particle systems. The obtained trajectories were further analyzed in MATLAB and details of the imaging process and analysis as well as the trajectory information are provided in the Supplementary Information. As noted earlier, the acquired trajectories were divided into three categories representing: i-mobile colloids, ii-remobilized colloids, and iii) permanently attached colloids (i.e., immobilized colloids). All trajectories describe the full path from the point of entry until the colloids either deposited or passed through the entire domain.

Using the obtained comprehensive information from experiments several transport properties were calculated including the tortuosity of particle trajectories, residence time of particles, frequency of attachment and remobilization events for each particle, as well as the penetration depth and the 1st and 2nd moments of the attached mass. Detailed information on the transport properties is provided in the Supplementary Materials.

2.4. Zeta potential

The zeta potential measurements were carried out with a Zetasizer Nano ZS analyser (Malvern Instruments, Worcestershire, UK). The colloid solution was prepared with a specific concentration in deionized water to measure the electrophoretic mobility of the dispersed colloids in solution. Before the measurements, the suspension was sonicated in an ultrasonic bath. Measurements were taken at 20 °C at neutral pH. The zeta potential was derived from the electrophoretic mobility assuming applicability of Henry's equation and Smoluchowski approximation (Sze et al., 2003) to calculate the DLVO forces. The equations to calculate the DLVO forces are given in the Supplementary Materials.

2.5. Breakthrough curve (BTC)

Traditionally, concentration breakthrough curves (i.e., BTCs) are measured at the outlet of the system by collecting the outflow solution. When using micromodel experiments, this is done by measuring fluorescence intensity at the outlet location of the domain (Zhang et al., 2015). The breakthrough curve shows an integrated, average, behavior of the system and does not uniquely reveal the contribution of the internal local behaviors. Nevertheless, BTC's are of importance for

upscaling using macroscopic continuum-scale modeling (Baumann and Werth, 2004). In our experiments, we simultaneously capture the internal pore-scale behavior of colloids as well as the average behavior which is obtained using the BTCs measured at the sample outlet.

3. Experimental results and analysis

Colloid transport experiments under unfavorable conditions resulted in a total of 1357 trajectories of the colloids, of which 1309 were transported through the entire domain without any deposition, 19 attached and then remobilized, and 29 colloids permanently attached to a collector surface. Fig. 3 shows the collection of trajectories that passed through the domain. While a large number of colloids percolated through the sample, we have observed several pores which never received any colloids. These pores are mainly dead-end pores and/or pores oriented perpendicular to the overall flow direction (-i.e., normal to the generated pressure gradients, leading to low flow velocities). In what follows, we first discuss the DLVO profile, next we focus on the integrated behavior of colloids in the system, followed by characterizing trajectories of the attached colloids, and the breakthrough curves.

3.1. DLVO profile

The measured zeta potential of the colloids in deionized water was −47 mV. The zeta potential for the PDMS was taken as −80 mV (Sze et al., 2003; Kirby and Hasselbrink, 2004; Almutairi et al., 2012) and the ionic strength close to zero. Fig. 4 shows that the DLVO profile between the colloids and the collector surface has a high primary minimum barrier, but no secondary minimum due to the low ionic strength. This
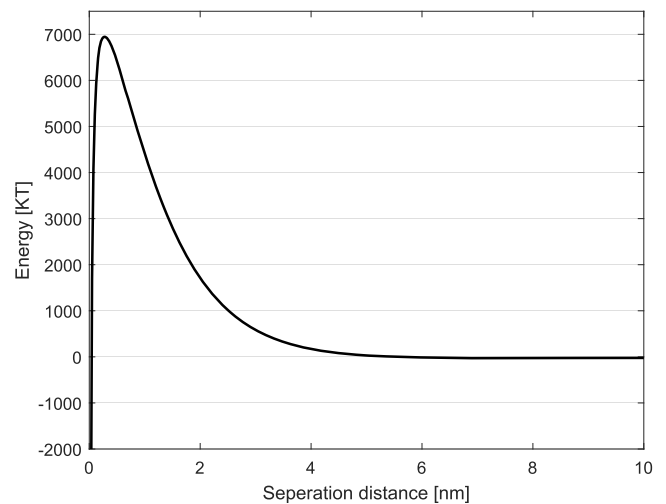

Fig. 4. DLVO energy profile between the collector surface (i.e., the micromodel PDMS solid grains) and colloid.

indicates unfavorable conditions under which colloid attachment is not probable when only DLVO forces were taken into consideration. However, several other processes could contribute to attachment including local grain roughness, surface charge heterogeneities, and local flow conditions (Bradford and Torkzaban, 2015; Bradford et al., 2015), which could lead to lower effective energy barrier and cause colloid attachment.
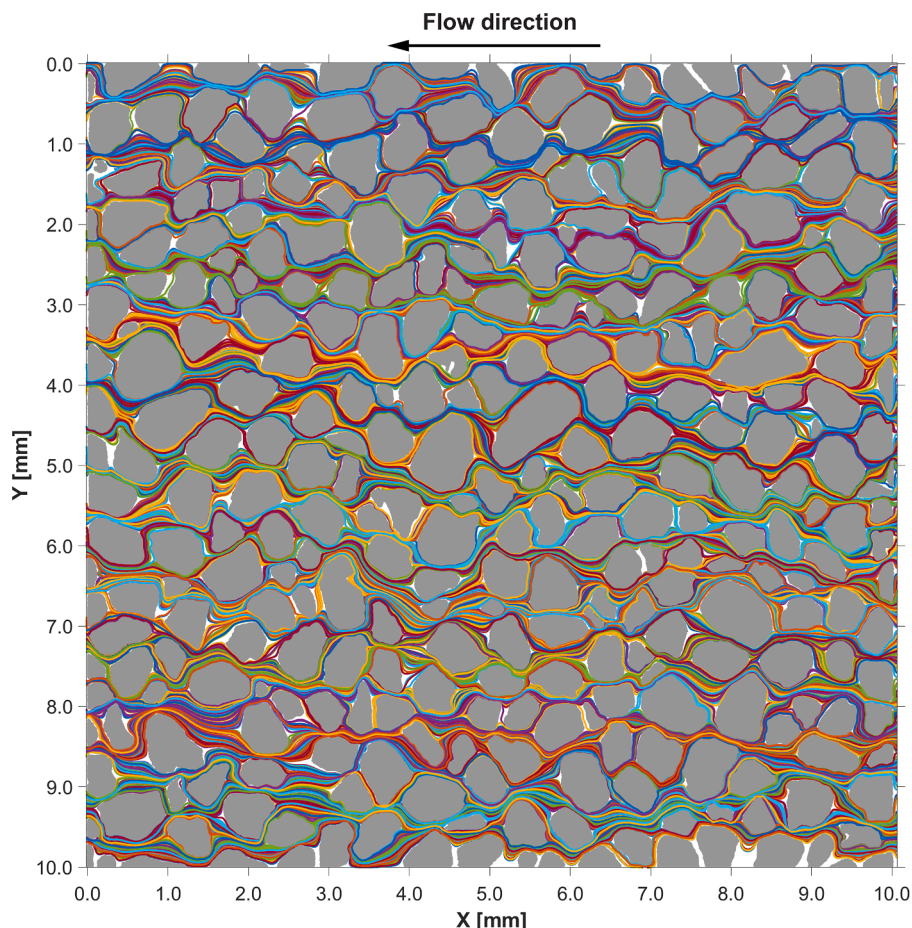

Fig. 3. Trajectories of all the colloids that were transported through the micromodel pore structures. Flow is from the right towards the left.

3.2. Tortuosity, normal distance to grain surface, and trajectory average velocity

Fig. 5 together with Table 2 (average values) show the behavior of colloid trajectories divided into three categories of mobile, remobilized and attached colloids. The probability distributions for the parameters are given in the Supplementary Materials. Results show that colloids that moved closer to the grain surfaces, had longer trajectories which increased their tortuosity (Fig. 5a), and caused lower observed transport velocities (Fig. 5b). Although data points are scattered in Fig. 5c, they show a general linear trend between the normal distance from the grains and the velocity of colloid trajectories. The outliers may be impacted by the measurement procedure (which is discussed in the Supplementary Materials). For colloids that were permanently attached inside the pore network, average values were calculated up to the moment of attachment. The attached colloids generally show transport at close distances to the solid grains, however they show a wide range of tortuosity values. When colloids were attached close to the inlet, the tortuosity of their trajectories remains close to 1.0 because of their short travel time and distance. The attached colloids which deposited at larger distances within the pore space showed higher tortuosity values mainly because they followed the curved grain surfaces during their transport.

Table 2
Average values of the tortuosity, distance from the grain surface, velocity of the trajectory, and the transport time in the domain for the three types of colloids categorized based on their behavior. Transport time for the attached particles refer to the elapsed time up to the moment of colloid attachment. The probability distributions are given in the Supplementary Materials.

Trajectory type	Tortuosity [−]	Distance to solid [m]	Velocity [ms⁻¹]	Transport time [s]
Mobile	1.205 (0.038)	5.692 $(1.060) \times 10^{-5}$	1.362 $(0.369) \times 10^{-4}$	92.4 (27.6)
Remobilized	1.225 (0.046)	5.057 $(1.565) \times 10^{-5}$	1.230 $(0.353) \times 10^{-4}$	144.4 (41.74)
Attached	1.200 (0.081)	4.445 $(1.199) \times 10^{-5}$	1.233 $(0.433) \times 10^{-4}$	59.2 (39.7)

Therefore, the average tortuosity of colloids that became permanently attached inside the domain can be even lower compared to other colloids. Remobilized colloids showed an average tortuosity value of 1.225 which is larger than the average tortuosity of mobile colloids (1.205). This is mainly because remobilized colloids follow more twisted paths during their relatively large residence times across the pore network. We can conclude that colloids subject to attachment have a higher tortuosity as they generally travel for longer times in the vicinity of solid surfaces
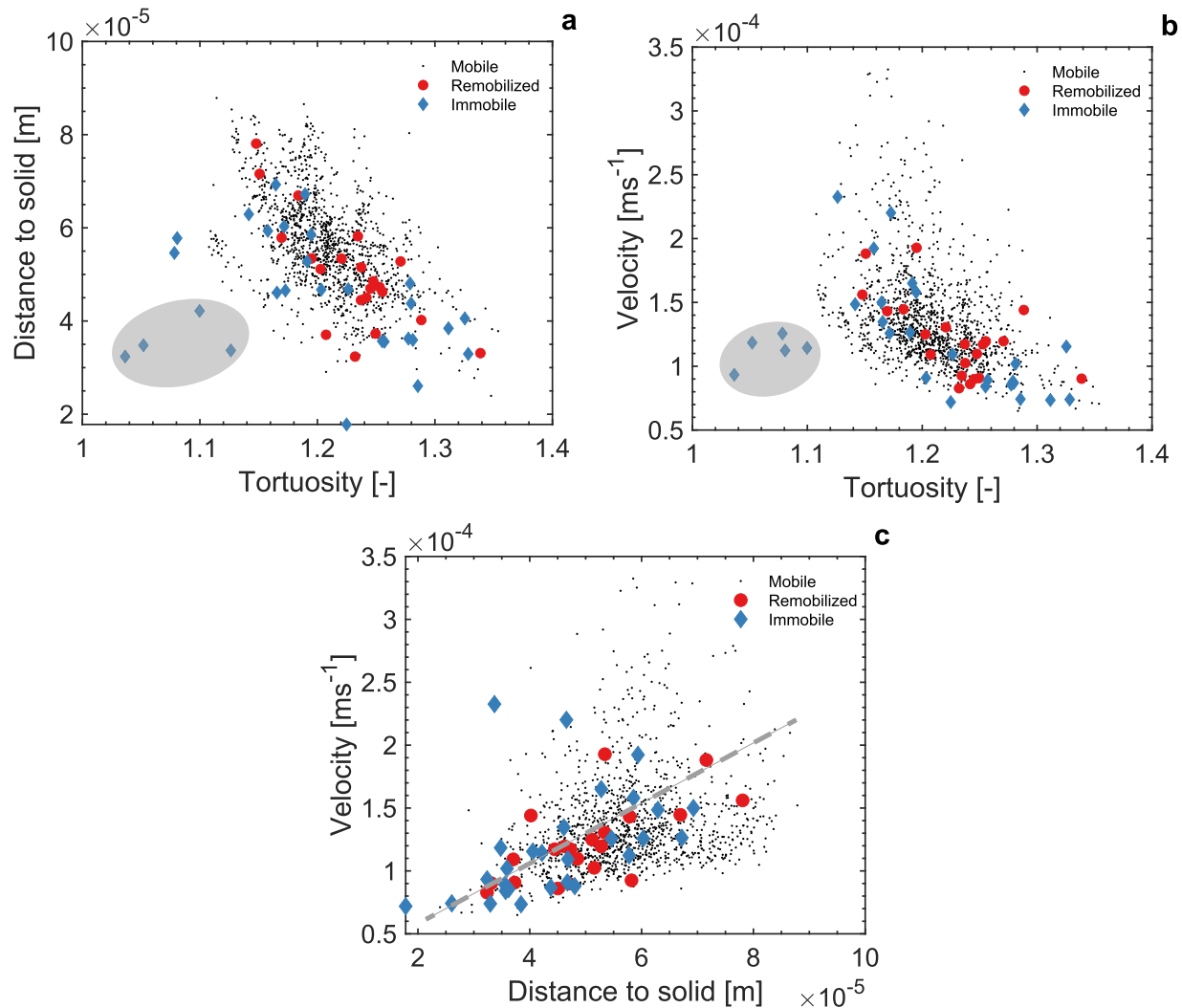

Fig. 5. Plots showing for each trajectory a) the average distance normal to the grain surfaces versus the tortuosity. b) average velocity versus tortuosity. c) average velocity versus the normal distance to the grain surfaces. Parameters for the attached particles (immobile) were calculated until the moment of attachment. The gray highlights indicate colloids that were attached soon after injection and therefore may have not experienced a sufficient fraction of domain pore structure. The probability distributions of the parameters are given in the Supplementary Materials.

and create longer paths compared to the colloids that were mobile and transported rather through the central regions of the pores.

Overall, the trajectory of remobilized and permanently attached colloids pass close to the grain surfaces, which causes the average velocity to be lower than the mobile colloids. Local variations in the flow velocity distribution and DLVO forces will determine the ultimate attachment of colloids.

3.3. Remobilization

In this section, we will describe colloid remobilization events. Of the trajectories that became permanently attached, none showed attachment and remobilization events before deposition, whereas 19 colloids showed attachment and remobilization. Below we will explore the average and standard deviation (i.e., sample scale) transport properties and then describe two of the trajectories in more detail. Analysis have been done on the temporal evolution of adsorption using the 1st and the 2nd moments which are given in the supplementary materials.

The remobilized colloids spent on average of 42.1 (48.5) s in the attached state (immobile), with the total time within the porous medium being on average 144.4 (41.74) s. This shows that the remobilized colloids spend, on average, 29% of the total residence time attached to the soil grains. This compares with mobile colloid which, on average, spend 92.4 (27.6) s within the domain. Comparing these residence times shows that remobilization requires on average 50% extra time for colloids to arrive at the outlet. The trajectories of these colloids have a higher tortuosity compared to the mobile colloids and they often are transported closer to the solid grains and have lower average velocities. In our experiments, the maximum time that a colloid was immobilized before being remobilized was 208 s, with this colloid residing 268 s inside the domain.

Typical examples of the colloid velocity and distance to solid against time are given in Fig. 6. We found that colloid 615 closely followed free flow (i.e., being mobile), while being transported only slightly closer to the walls compared to the completely mobile colloids. Before attachment, the colloids came closer to the collector surface before being immobile for 110 s. While being immobile, the colloid showed very little movement although very small fluctuations in the velocity are visible (the velocities fall within the error margin, an assessment is made in the Supplementary Materials). Colloid 548 also follows a free flow path before reaching a low-velocity area where it is immobilized for 10 s. After remobilization, the colloid shows rolling along the collector surface before it is transported by bulk free flow. Similar behavior was

found for the 18 other colloids that showed attachment and remobilization.

In this study only forward flow was applied and the results showed remobilization of colloids, either by local flow velocity perturbations or rolling along the surface at very low rates. While other mechanisms could lead to remobilization as well, i.e.- increased flow velocity (Bradford et al., 2009; Knappenberger et al., 2014), moving interfaces (Aramrak et al., 2011; Zhang et al., 2013), shift in chemical conditions (Mitropoulou et al., 2013; Samari-Kermani et al., 2021), or reversed flow (Reichhardt and Reichhardt, 2018).

3.4. Permanently attached colloids

Fig. 7 shows the location of the attached colloids together with their trajectories (before attachment) inside the transport domain. Additionally, Table 3 provides the average properties of the attached colloids. Fig. 7 shows that although most of colloids were attached to the solid grain walls, some of them were attached to the top or bottom section of the microfluidic. The mean throat size in which colloid attachment has occurred is 0.107 mm (probability density function is given in the supplementary materials), and the average throat size of the domain is 0.145 mm. Therefore, colloids have shown tendency to become attached within the smaller pores. In several cases, multiple colloids were attached at the same location. When this occurs, the first attached colloid may turn the situation more favorable for the newly arriving colloids to attach (shown by blue markers in Fig. 7).

The peak arrival time of mobile colloid concentration at the outlet was 90 s. However, a small fraction of colloids became attached at time later than 100 s. These colloids mostly attached in regions close to the end of the domain and often had a lower average velocity compared the bulk flow. Travel times much higher than those of the mobile colloids would indicate a high amount of remobilization occurring in the system. However, our results show that the attached colloids were not subject to remobilization prior to permanent attachment. Furthermore, from Fig. 7 it is evident that several colloids move for some time in close proximity to the collector surface prior to attachment. This behavior shows that the attraction forces are relatively weak to hold the colloids strongly, and that it takes some time for colloids to find an attachment location where the net forces are favorable for attraction.

Fig. 8 shows the trajectories of three colloids. Even though colloid 1290 was attached and the other two colloids were mobile throughout the flow domain, however all three had very similar trajectories during most of their flow path. Colloid 1280 reached a low-velocity zone after
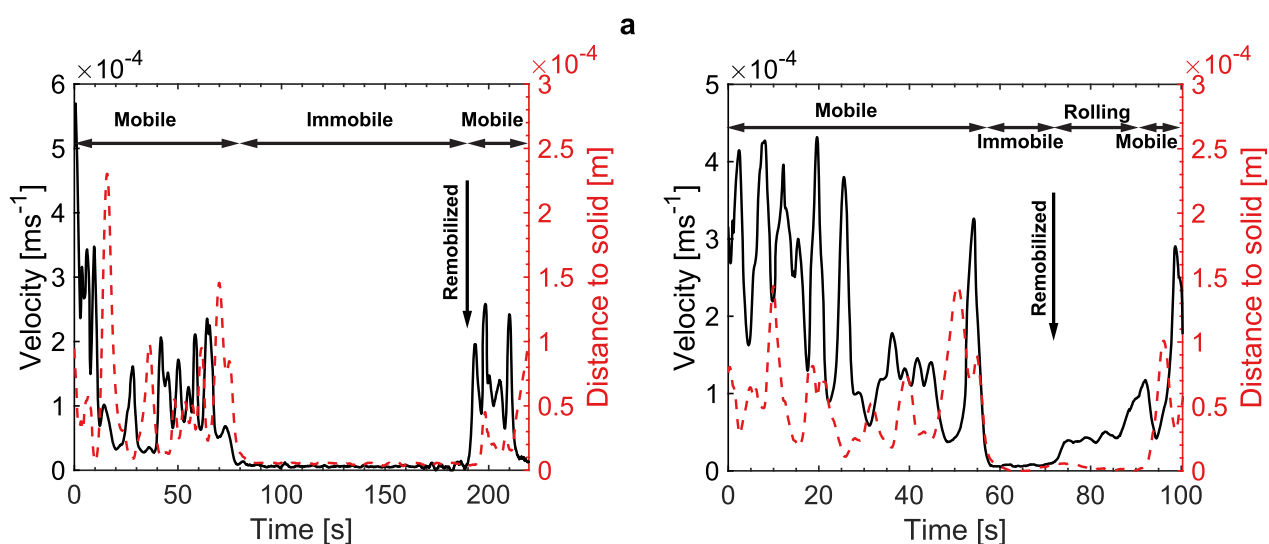

Fig. 6. Plots showing for colloids 610 (a) and 548 (b) their velocity (left y-axes) and distance to the solid grains (right y-axes) over time. Colloid 615 colloid showed attachment for a duration of 110 s before being remobilized and colloid 548 which showed attachment for a total duration of 10 s.
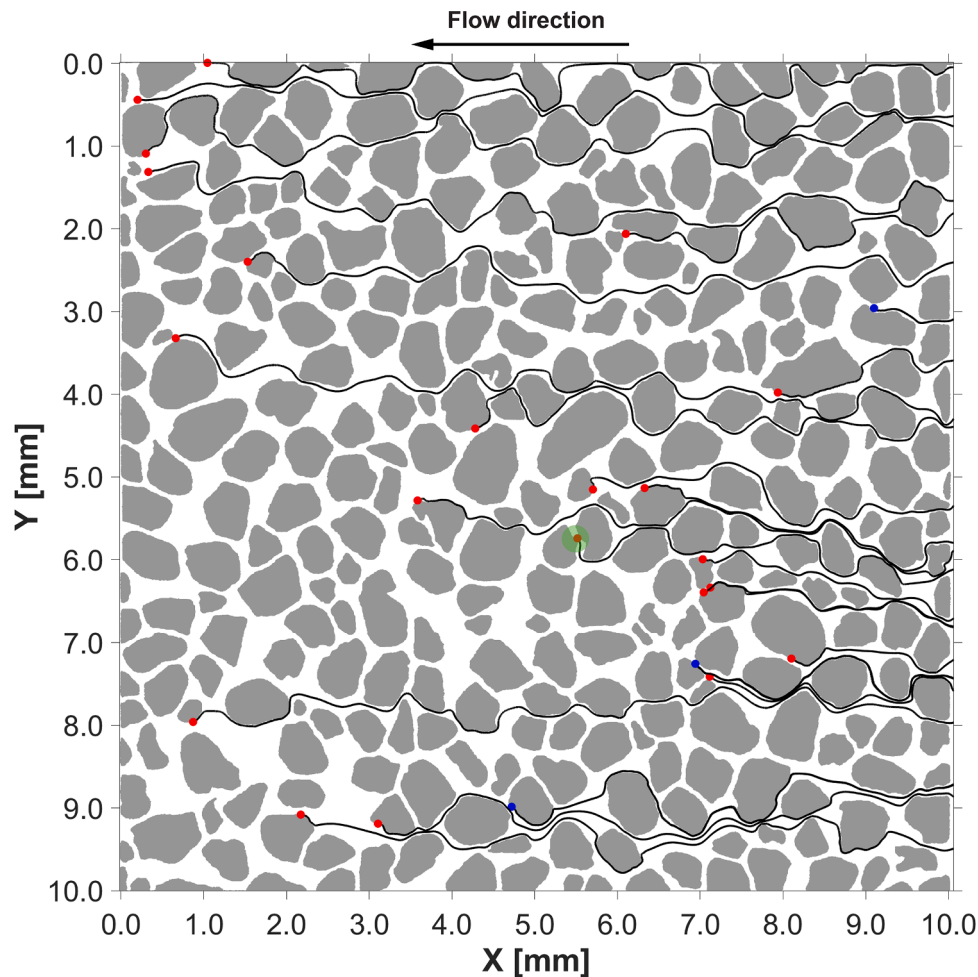
Flow direction

Fig. 7. Trajectories of the attached colloids. The blue markers indicate locations where more than one colloid were attached, and the red markers locations where a single colloid was attached. The colloid marked by a green circle was attached in a pore orientated perpendicular to the general flow direction.

Table 3
Average properties of attached particle trajectories.

Property	Value
Penetration depth [m]	$5.185\ (2.905)\times10^{-3}$
Displacement till attachment [m]	$6.319\ (3.539)\times10^{-3}$
Tortuosity till attachment [−]	1.200 (0.081)
Time till attachment [s]	59.2 (39.7)
Mean pore body size at attachment [m]	$3.183\ (1.102)\times10^{-4}$
Mean pore throat size at attachment [m]	$1.069\ (0.819)\times10^{-4}$

100 s when it began rolling along the surface for another 70 s before attachment. Rolling of the colloid was due to the overall unfavorable conditions for attachment where colloids can attach at a smaller fraction of surfaces when a suitable site is found and the energy barrier is lower due to local roughness, chemical heterogeneities, and/or lower local fluid flow velocities.

Fig. 8c shows the velocity profile (i.e., along the sample) for an ultimately attached colloid (number 1280) as well as for another two trajectories passing through the whole domain without any deposition. Although the trajectories (shown in Fig. 8a) were very similar, the velocity distribution was different for each track. Until 9.5 mm, there was no indication that track 1278 would become attached. At 9.5 mm, the particle stagnates and rolled until becoming attached. This observation reveals the challenge of using the location and shape of a trajectory to predict whether an attachment event will occur.

3.5. Bridging

Colloid sizes and surface properties together with a relatively low input concentration of colloids (which is often the case in subsurface environments) used in this study resulted in no straining, clogging, or aggregation in our experiments. However, local colloid bridging was observed at three locations where attachment took place in proximity of a previous attached colloid. We should note that as bridging happens and more colloids attach at the same location, the emission from the fluorescence particles intensifies, but the resolution limit makes it difficult to distinguish each particle after they are attached. Nevertheless, because of the trajectory that leads exactly to the previously attached particle (see Fig. 7, blue dots and their trajectories), we could detect the bridging process. Fig. 9 shows the velocity of this category of colloids versus the longitudinal distance. While the three trajectories were similar, the transport velocities were different between these trajectories. At location 0.25 mm, we observed the highest velocity reached by colloid 402, and followed by colloids 883 and 1246. While at location 2.1 mm we observed the highest velocity reached by colloid 1246, and subsequently by 883 and 402. This indicates that the correlation of transport velocity between pores is relatively low, which is often assumed to occur up to one pore (Alim et al., 2017; Miele et al., 2019). It is difficult to foresee if a particle will bridge to another particle, although the trajectories indicate that the flow velocities do not differentiate much between the trajectories. This also indicates that the colloids were probably being transported at similar depth inside the micromodel, and thus making it more likely to bridge to a previously attached colloid.
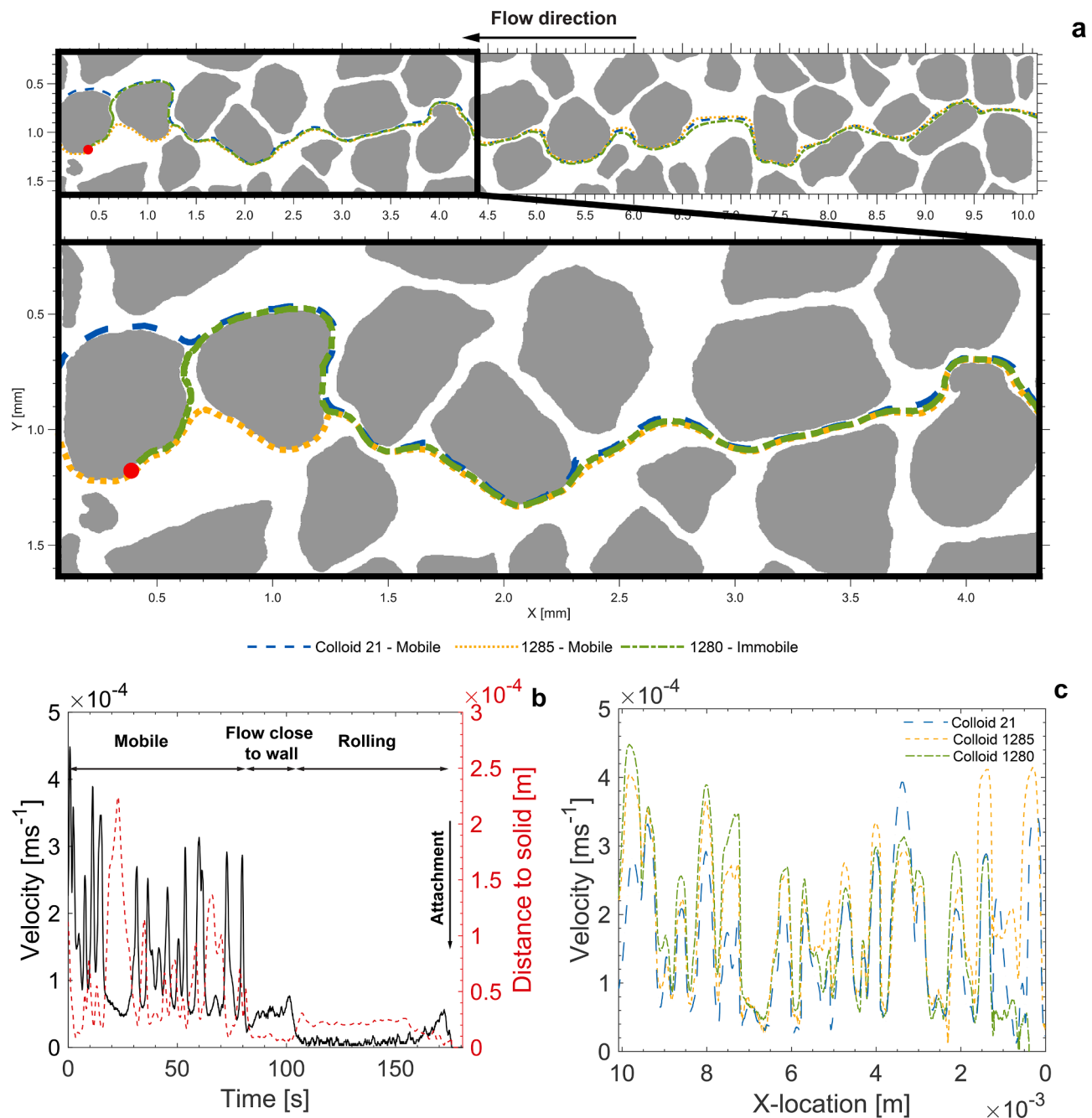
Fig. 8. a) Trajectories of colloid number 1280 (as an attached (immobile) colloid) and colloids number 1285 and 21 (as mobile colloids), shown in full length as well as a zoomed in section. The two trajectories followed similar pathway through most of the domain, and the trajectory of the attached particle changed near the end of the flow domain where it attached. b) Plots of the velocity and distance to the solid grains against time for colloid 1280, showing that prior to attachment this colloid was rolling over the solid surface. c) Plots of the colloid velocity against location for colloids 1280 (attached) and 1285 and 21 (mobile).

3.6. Breakthrough curves

A major aim of this study was to capture full colloid trajectories throughout the domain, as well as colloid concentrations at the outlet to provide insight into the breakthrough curves. Our micromodel was designed to have a uniform flux at the inlet of the sample. However, small discrepancies between the inlet channels were inevitable. This will cause slight local differences in the velocity field and fluctuations in arrival times of colloids at the start of the pore network. Moreover, hydrodynamic dispersion will likely occur also inside the inlet tube, as well as inside the inlet channels of the micromodel. These factors will turn the pulse input into a distributed and often skewed input concentration which may fluctuate over time. However, since the whole pore space was imaged, the arrival time of each individual colloid at the start of the pore domain and when they surpass the outlet, which corresponds to the residence time in the pore network of the colloid. We can normalize colloid entrance times and construct a Dirac delta input (i.e., in the normalized form all the particles enter the domain instantaneously at $t = 0$) which is equal to the probability density function of the residence time.

Constructing the breakthrough curve in this way would assure that colloids migrate and interact with the solid grain individually (i.e., no dominant colloid-colloid interaction) which is valid for our experiments based on our observations of colloid trajectories. Having the information
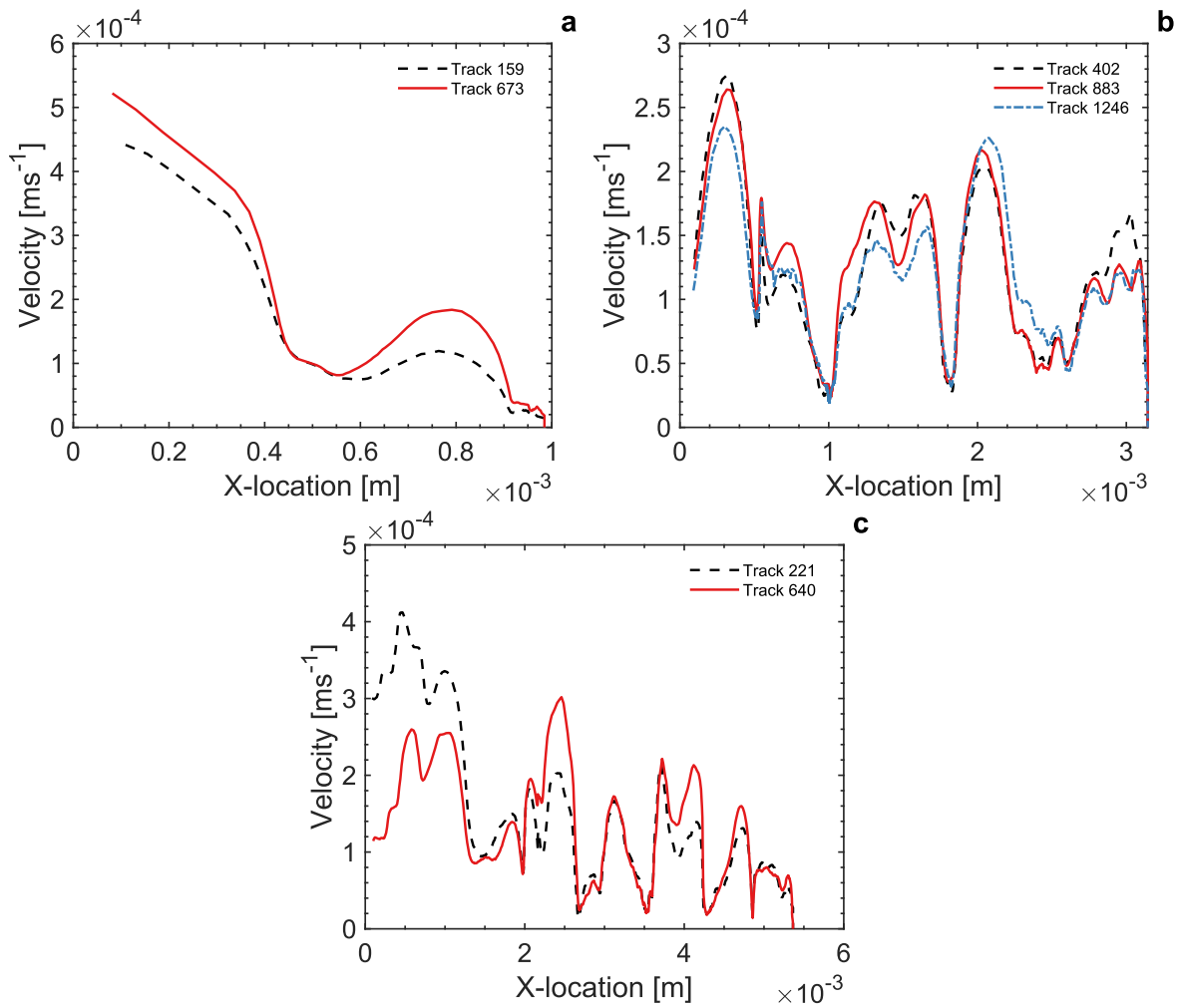
Fig. 9. Colloid velocities along the longitudinal distance for colloids that were attached (immobilized) at the same location. a) Colloids 159 and 673, b) colloids 402, 883, and 1246, c) colloids 221, and 640.

of full trajectories for different categories of colloids, we can construct various breakthrough curves from one dataset, such as BTC of all colloids entered the system, BTC of mobile colloids, and BTC of colloids only with detachment and/or remobilization events. This will a much better understanding of the influence of attachment and remobilization on the breakthrough curves.
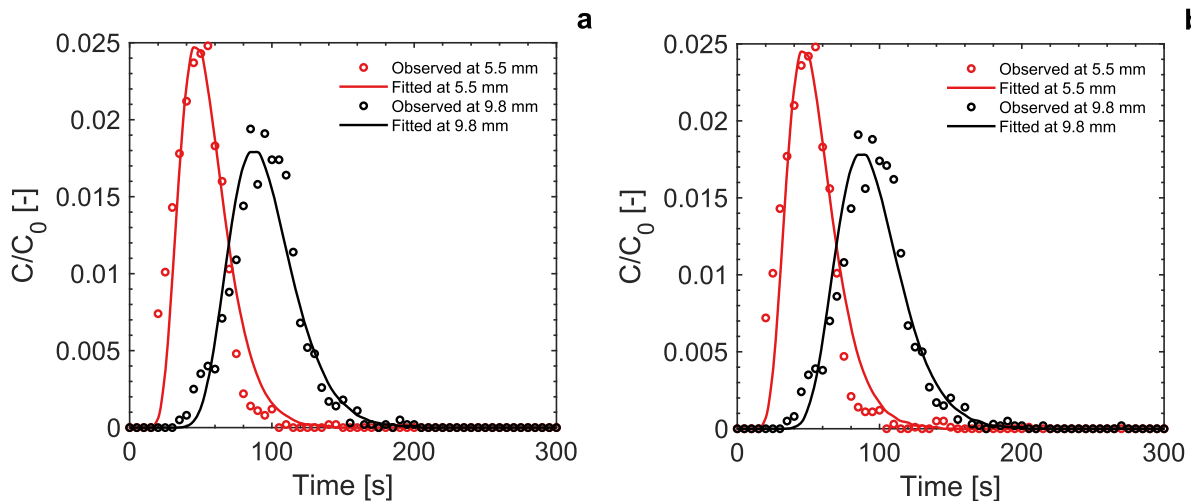

Fig. 10. Dirac delta input breakthrough curves and the multi-fit results. a) Colloids that were mobile during their transport through the pore domain, breakthrough at multiple locations (mm) through the domain. b) All Colloids that were transported through the pore domain, breakthrough at multiple locations (mm) through the domain.

Fig. 10 shows the normalized average concentration breakthrough curves (BTCs) for colloids that were mobile in the domain and for all colloids. The progression of colloids within the domain in form of concentration BTCs are given in Supplementary Materials. Due to the small number of particles with attachment and detachment events (compared to the bulk flow) we see little influence on the shape of the obtained breakthrough curves. All curves are only slightly asymmetrical which is due to the preferential (nonequilibrium) flow paths, with colloid attachment/detachment causing slight increase in late-time tailing of the BTCs. When we exclude these processes, one can analyze the obtained BTCs in terms of the classic Advection-Dispersion Equation, ADE $\left(\frac{\partial c}{\partial t} = D \frac{\partial^2 c}{\partial x^2} - v \frac{\partial c}{\partial x} \right)$, where C represents the colloid concentration, v denotes the pore water velocity, D is the dispersion coefficient, t is time, and x is the spatial coordinate as before. It is also possible to use a Advection-Dispersion-Sorption equation, for example a one-site or two-site kinetic model, to account for the sorption and desorption of colloids to and from the solid wall (Schijven and Šimrunek, 2002; Molnar et al., 2015). For example, if the fraction of remobilized and attached colloids would increase, which have longer residence time than the mobile colloids, then the traditional ADE would not suit for the observed BTC. In this case, we chose to analyze both trajectory categories using the equilibrium ADE as its was adequate to describe the observed attachment/detachment processes. Fig. 10 shows the multi fitted BTCs (single fit results are provided in Supplementary Materials) and Table 4 provides the optimized transport parameters (D, v, and the dispersivity, $\alpha = Dv$) obtained by CXTIFIT code in STANMOD (Šimůnek et al., 1999), as well the R^2 values for a single fit at only the location of 9.8 mm and a multi-fit where the transport parameters were optimized simultaneously for BTCs at two locations (i.e., $x = 5.5$ and 9.8 mm). The single fits performed slightly better indicated by the R^2 value, and the fitted velocities are marginally lower than those obtained using the multi-fit. The fitted velocities are slightly lower than the estimated values as shown in Table 2. The underestimation can be caused by the presence of the preferential flow paths. The dispersion coefficient for multi-fit optimization is higher than the single fit which is due to the stronger bell shape of the fitted BTCs (Supplementary materials). Results show the influence of the attachment, attachment/detachment trajectories on the BTCs as slightly higher estimated dispersion coefficient, and hence also the dispersivity value.

4. Conclusions

In this study we have developed a new microscopy setup to perform colloidal experiments at the cm scale, while simultaneously observing transport, attachment, and remobilization of all individual colloids at the micrometer scale. For each individual colloid that was transported through the domain, the trajectory was captured and analyzed to explore the attachment. We found that even under unfavorable conditions, based on the DLVO interactions, colloids were attached due to fluctuations in the local flow velocity (i.e., fluctuating hydrodynamic forces and local roughness affecting local DLVO forces). The observed trajectories were normalized into single breakthrough curves and fitted using analytical solutions which describes colloids transport as 1D macroscopic process along the general flow direction. This study as particularly showed that:

- The trajectory of the remobilized and permanently attached colloids overall passed close to the grain surfaces with a lower average velocity compared to the velocity of the bulk flow.
- Due to low input concentration no colloid aggregation was observed and therefore straining was not observed due to the low ratio in particle size versus the pore sizes. A few instances of bridging were observed, this retention processes, as well as straining would be expected to be a higher contributor to retention at higher input concentrations.

Table 4
Optimized ADE transport parameters for mobile colloids and all colloids combined. The single fit belongs to the breakthrough curve at 9.8 mm, and the multifit for simultaneous analysis of the breakthrough curves at 5.5 mm and 9.8 mm.

Trajectory type Fitting Method	Mobile colloids Single fit	Multi fit	All colloids Single fit	Multi fit
V [ms^{-1}]	1.02×10^{-4}	1.06×10^{-4}	1.02×10^{-4}	1.06×10^{-4}
D [m^{2}s^{-1}]	2.58×10^{-8}	3.23×10^{-8}	2.64×10^{-8}	3.27×10^{-8}
α [m]	2.53×10^{-4}	3.05×10^{-4}	2.59×10^{-4}	3.10×10^{-4}
R^2	0.964	0.941	0.964	0.940

- The remobilized colloids spent, on average, 29% of the total residence time in the attached state at the soil grains.
- After remobilization, some colloids show rolling along the collector surface before being transported into the bulk free flow.
- Colloids with very similar trajectories (i.e., transportation in close vicinity of each other) could show different attachment behaviors and different flow velocities along their respective trajectories.
- Attached colloids showed clear rolling over the solid grains, due to the overall unfavorable conditions for attachment before their depositions.
- Attachment and remobilization caused slight increase in estimated dispersion coefficient, and subsequently the dispersivity value of the media, obtained by fitting to the ADE equation.

The developed microscopic set-up demonstrates the potential to further investigate pore-scale behavior at the cm scale by including various chemical conditions, hydrophobicity changes, flow conditions, two-phase flow, colloid size and shape, and different pore structure topologies. Furthermore, the set-up can be extended with an additional camera and light source to be able to observe two different species of colloids simultaneously, or of colloids together with a fluorescent dye to capture their interactions.

CRediT authorship contribution statement

Enno T. de Vries: Conceptualization, Methodology, Investigation, Data curation, Software, Formal analysis, Writing – original draft. **Qianjing Tang:** Conceptualization, Investigation. **Sanli Faez:** Supervision, Writing – review & editing. **Amir Raoof:** Supervision, Writing – review & editing, Funding acquisition.

Declaration of Competing Interest

The authors declare that they have no known competing financial interests or personal relationships that could have appeared to influence the work reported in this paper.

Supplementary materials

Supplementary material associated with this article can be found, in the online version, at doi:10.1016/j.advwatres.2021.104086.

References

Alim, K., Parsa, S., Weitz, D.A., Brenner, M.P., 2017. Local pore size correlations determine flow distributions in porous media. Phys. Rev. Lett. 119 (14), 144501 https://doi.org/10.1103/physrevlett.119.144501.

Almutairi, Z., Ren, C.L., Simon, L., 2012. Evaluation of polydimethylsiloxane (PDMS) surface modification approaches for microfluidic applications. Colloids Surf. A 415, 406–412. https://doi.org/10.1016/j.colsurfa.2012.10.008.

Aramrak, S., Flury, M., Harsh, J.B., 2011. Detachment of deposited colloids by advancing and receding air-water interfaces. Langmuir 27 (16), 9985–9993. https://doi.org/10.1021/la201840q.

Argent, J., Torkzaban, S., Hubbard, S., Le, H., Amirianshoja, T., Haghighi, M., 2015. Visualization of micro-particle retention on a heterogeneous surface using micro-models: influence of nanoscale surface roughness. Transp. Porous Med. 109 (2), 239–253. https://doi.org/10.1007/s11242-015-0511-z.

Auset, M., Keller, A.A., 2006a. Pore-scale visualization of colloid straining and filtration in saturated porous media using micromodels. Water Resour. Res. 42 (12) https://doi.org/10.1029/2005wr004639.

Auset, M., Keller, A.A., 2006b. Pore-scale visualization of colloid straining and filtration in saturated porous media using micromodels. Water Resour. Res. 42 (12) https://doi.org/10.1029/2005wr004639.

Baumann, T., Werth, C.J., 2004. Visualization and Modeling of Polystyrol Colloid Transport in a Silicon Micromodel. Vadose Zone J. 3 (2), 434–443. https://doi.org/10.2136/vzj2004.0434.

Bradford, S.A., Torkzaban, S., 2015. Determining Parameters and Mechanisms of Colloid Retention and Release in Porous Media. Langmuir 31 (44), 12096–12105. https://doi.org/10.1021/acs.langmuir.5b03080.

Bradford, S.A., Torkzaban, S., Leij, F., Šimnek, J., Genuchten, M.T.v., 2009. Modeling the coupled effects of pore space geometry and velocity on colloid transport and retention. Water Resour. Res. 45 (2) https://doi.org/10.1029/2008wr007096.

Bradford, S.A., Torkzaban, S., Leij, F., Simunek, J., 2015. Equilibrium and kinetic models for colloid release under transient solution chemistry conditions. J. Contam. Hydrol. 181 (44), 141–152. https://doi.org/10.1016/j.jconhyd.2015.04.003.

Jaqaman, K., Loerke, D., Mettlen, M., Kuwata, H., Grinstein, S., Schmid, S.L., Danuser, G., 2008. Robust single-particle tracking in live-cell time-lapse sequences. Nat. Methods 5 (8), 695–702. https://doi.org/10.1038/nmeth.1237.

Kirby, B.J., Hasselbrink, E.F., 2004. Zeta potential of microfluidic substrates: 2. Data for polymers. Electrophoresis 25 (2), 203–213. https://doi.org/10.1002/elps.200305755.

Knappenberger, T., Flury, M., Mattson, E.D., Harsh, J.B., 2014. Does Water Content or Flow Rate Control Colloid Transport in Unsaturated Porous Media? Environ. Sci. Technol. 48 (7), 3791–3799. https://doi.org/10.1021/es404705d.

Kretzschmar, R., Borkovec, M., Grolimund, D., Elimelech, M., 1999. Mobile Subsurface Colloids and Their Role in Contaminant Transport. Advances in Agronomy 66, 121–193. https://doi.org/10.1016/s0065-2113(08)60427-7.

Kretzschmar, R., Schafer, T., 2005. Metal Retention and Transport on Colloidal Particles in the Environment. Elements 1 (4), 205–210. https://doi.org/10.2113/gselements.1.4.205.

Lazouskaya, V., Wang, L.-.P., Gao, H., Shi, X., Czymmek, K., Jin, Y., 2011. Pore-Scale Investigation of Colloid Retention and Mobilization in the Presence of a Moving Air-Water Interface. Vadose Zone J. 10 (4), 1250–1260. https://doi.org/10.2136/vzj2011.0003.

Lazouskaya, V., Wang, L.-.P., Or, D., Wang, G., Caplan, J.L., Jin, Y., 2013. Colloid mobilization by fluid displacement fronts in channels. J. Colloid Interface Sci. 406, 44–50. https://doi.org/10.1016/j.jcis.2013.05.078.

Lindeberg, T., 1998. Feature Detection with Automatic Scale Selection. Int J Comput Vis 30 (2), 79–116. https://doi.org/10.1023/a:1008045108935.

Liu, Q., Zhao, B., Santamarina, J.C., 2019. Particle Migration and Clogging in Porous Media: a Convergent Flow Microfluidics Study. J. Geophys. Res.: Solid Earth, 124 (9), 9495–9504. https://doi.org/10.1029/2019jb017813.

Massoudieh, A., & Ginn, T.R. (2010). Colloid-Facilitated Contaminant Transport in Unsaturated Porous Media. (G. Hanrahan, Ed.)Modelling of Pollutants in Complex Environmental Systems. ILM Publications.

Miele, F., Anna, P.d.e., Dentz, M., 2019. Stochastic model for filtration by porous materials. Phys. Rev. Fluids 4 (9). https://doi.org/10.1103/physrevfluids.4.094101.

Mitropoulou, P.N., Syngouna, V.I., Chrysikopoulos, C.V., 2013. Transport of colloids in unsaturated packed columns: role of ionic strength and sand grain size. Chem. Eng. J. 232, 237–248. https://doi.org/10.1016/j.cej.2013.07.093.

Molnar, I.L., Gerhard, J.I., Willson, C.S., OtextquotesingleCarroll, D.M., 2015a. The impact of immobile zones on the transport and retention of nanoparticles in porous media. Water Resour. Res. 51 (11), 8973–8994. https://doi.org/10.1002/2015wr017167.

Molnar, I.L., Johnson, W.P., Gerhard, J.I., Willson, C.S., OtextquotesingleCarroll, D.M., 2015b. Predicting colloid transport through saturated porous media: a critical review. Water Resour. Res. 51 (9), 6804–6845. https://doi.org/10.1002/2015wr017318.

Nguyen, H.T., Reichhardt, C., Reichhardt, C.J.O., 2017. Clogging and jamming transitions in periodic obstacle arrays. Phys. Rev. E 95 (3), 030902. https://doi.org/10.1103/physreve.95.030902.

Parvan, A., Jafari, S., Rahnama, M., Norouzi-Apourvari, S., Raoof, A., 2021. Insight into particle detachment in clogging of porous media; a pore scale study using lattice Boltzmann method. Adv Water Resour. 151, 103888 https://doi.org/10.1016/j.advwatres.2021.103888.

Pekdeger, A., Matthess, G., 1983. Factors of bacteria and virus transport in groundwater. Environ. Geol. 5 (2), 49–52. https://doi.org/10.1007/bf02381095.

Peng, Z., Doroodchi, E., Evans, G., 2010. DEM simulation of aggregation of suspended nanoparticles. Powder Technol. 204 (1), 91–102. https://doi.org/10.1016/j.powtec.2010.07.023.

Péter, H., Libál, A., Reichhardt, C., Reichhardt, C.J., 2018. Crossover from jamming to clogging behaviours in heterogeneous environments. Sci. Rep. 8 (1), 1–9. https://doi.org/10.1038/s41598-018-28256-6.

Reichhardt, C., Reichhardt, C., 2018. Controlled Fluidization, Mobility, and Clogging in Obstacle Arrays Using Periodic Perturbations. Phys. Rev. Lett. 121 (6), 068001 https://doi.org/10.1103/physrevlett.121.068001.

Reichhardt, C., Reichhardt, C.J.O., 2017. Negative differential mobility and trapping in active matter systems. J. Phys. Condens. Matter 30 (1), 015404. https://doi.org/10.1088/1361-648x/aa9c5f.

Reichhardt, C., Reichhardt, C.J.O., 2021. Directional clogging and phase separation for disk flow through periodic and diluted obstacle arrays. Soft Matter 17 (6), 1548–1557. https://doi.org/10.1039/d0sm01714k.

Rodrigues, S.M., Trindade, T., Duarte, A.C., Pereira, E., Koopmans, G.F., Römkens, P.F.A. M., 2016. A framework to measure the availability of engineered nanoparticles in soils: trends in soil tests and analytical tools. Trends Anal. Chem. 75, 129–140. https://doi.org/10.1016/j.trac.2015.07.003.

Ryan, J.N., Elimelech, M., 1996. Colloid mobilization and transport in groundwater. Colloids Surf. A 107, 1–56. https://doi.org/10.1016/0927-7757(95)03384-x.

Samari-Kermani, M., Jafari, S., Rahnama, M., Raoof, A., 2021. Ionic strength and zeta potential effects on colloid transport and retention processes. Colloid Interface Sci. Commun. 42, 100389 https://doi.org/10.1016/j.colcom.2021.100389.

Sang, W., Morales, V.L., Zhang, W., Stoof, C.R., Gao, B., Schatz, A.L., Zhang, Y., 2013. Quantification of Colloid Retention and Release by Straining and Energy Minima in Variably Saturated Porous Media. Environ. Sci. Technol. 47, 8256–8264. https://doi.org/10.1021/es400288c.

Schijven, J.F., Hassanizadeh, S.M., 2000. Removal of viruses by soil passage: overview of modeling, processes, and parameters. Crit. Rev. Environ. Sci. Technol. 30 (1), 49–127. https://doi.org/10.1080/10643380091184174.

Schijven, J.F., Šimrunek, J., 2002. Kinetic modeling of virus transport at the field scale. J. Contam. Hydrol. 55 (1–2), 113–135. https://doi.org/10.1016/s0169-7722(01)00188-7.

Šimůnek, J., Van Genuchten, M.T., Šejna, M., Toride, N., Leij, F.J., 1999. The STANMOD computer software for evaluating solute transport in porous media using analytical solutions of convection-dispersion equation. Rep. IGWMC-TPS 71 (32).

Sun, J., Tandogan, N., Gu, A.Z., Müftü, S., Goluch, E.D., Wan, K.-.T., 2018. Quantification of colloidal filtration of polystyrene micro-particles on glass substrate using a microfluidic device. Colloids Surf. B 165, 381–387. https://doi.org/10.1016/j.colsurfb.2018.02.044.

Syngouna, V.I., Chrysikopoulos, C.V., 2015. Experimental investigation of virus and clay particles cotransport in partially saturated columns packed with glass beads. J. Colloid Interface Sci. 440, 140–150. https://doi.org/10.1016/j.jcis.2014.10.066.

Sze, A., Erickson, D., Ren, L., Li, D., 2003. Zeta-potential measurement using the Smoluchowski equation and the slope of the current-time relationship in electroosmotic flow. J. Colloid Interface Sci. 261 (2), 402–410. https://doi.org/10.1016/s0021-9797(03)00142-5.

Tinevez, J.-.Y., Perry, N., Schindelin, J., Hoopes, G.M., Reynolds, G.D., Laplantine, E., Bednarek, S.Y., 2017. TrackMate: an open and extensible platform for single-particle tracking. Methods 115, 80–90. https://doi.org/10.1016/j.ymeth.2016.09.016.

Troester, M., Brauch, H.-.J., Hofmann, T., 2016. Vulnerability of drinking water supplies to engineered nanoparticles. Water Res. 96, 255–279. https://doi.org/10.1016/j.watres.2016.03.038.

Tufenkji, N., Elimelech, M., 2004. Deviation from the Classical Colloid Filtration Theory in the Presence of Repulsive DLVO Interactions. Langmuir 20 (25), 10818–10828. https://doi.org/10.1021/la0486638.

Wang, C., Bobba, A.D., Attinti, R., Shen, C., Lazouskaya, V., Wang, L.-.P., Jin, Y., 2012. Retention and Transport of Silica Nanoparticles in Saturated Porous Media: effect of Concentration and Particle Size. Environ. Sci. Technol. 46 (13), 7151–7158. https://doi.org/10.1021/es300314n.

Wang, M., Gao, B., Tang, D., 2016. Review of key factors controlling engineered nanoparticle transport in porous media. J. Hazard. Mater. 318, 233–246. https://doi.org/10.1016/j.jhazmat.2016.06.065.

Wang, Q., Lee, J.-.H., Jeong, S.-.W., Jang, A., Lee, S., Choi, H., 2011. Mobilization and deposition of iron nano and sub-micrometer particles in porous media: a glass micromodel study. J. Hazard. Mater. 192 (3), 1466–1475. https://doi.org/10.1016/j.jhazmat.2011.06.066.

Yao, K.-.M., Habibian, M.T., O'Melia, C,R., 1971. Water and waste water filtration. Concepts and applications. Environ. Sci. Technol. 5 (11), 1105–1112. https://doi.org/10.1021/es60058a005.

Zhang, Q., Hassanizadeh, S.M., Karadimitriou, N.K., Raoof, A., Liu, B., Kleingeld, P.J., Imhof, A., 2013. Retention and remobilization of colloids during steady-state and transient two-phase flow. Water Resour. Res. 49 (12), 8005–8016. https://doi.org/10.1002/2013WR014345.

Zhang, Q., Raoof, A., Hassanizadeh, S.M., 2015. Pore-Scale Study of Flow Rate on Colloid Attachment and Remobilization in a Saturated Micromodel. J. Environ. Qual. 44 (5), 1376. https://doi.org/10.2134/jeq2015.01.0058.

Zhou, J., Liu, D., Zhang, W., Chen, X., Huan, Y., Yu, X., 2017. Colloid characterization and in situ release in shallow groundwater under different hydrogeology conditions. Environ.Sci. Pollut. Res. 24 (16), 14445–14454. https://doi.org/10.1007/s11356-017-8856-1.